PAPER

Check for updates

A cooperative model for metallocene catalyst activation by methylaluminoxane†

Scott Collins* and Mikko Linnolahti [ID] *

Activation of rac-Me$_2$Si(η^5-Ind)$_2$ZrMe$_2$ (SBIZrMe$_2$) and sheet models for MAO, (MeAlO)$_6$(Me$_3$Al)$_4$ (6,4), (MeAlO)$_7$(Me$_3$Al)$_5$ (7,5), and (MeAlO)$_{26}$(Me$_3$Al)$_9$ (26,9) was studied via DFT. These activators can reversibly form an outer-sphere ion-pair (OSIP) [SBIZrMe$_2$AlMe$_2$] [(MeAlO)$_n$(Me$_3$Al)$_m$Me] **3** ([n,m]$^-$ = [7,4]$^-$and [26,8]$^-$) or a contact ion-pair (CIP) SBIZrMe-μ-Me-6,4 (**2b**) from SBIZrMe$_2$. Dissociation of Me$_3$Al from **3** to form CIP SBIZrMe-μ-Me-n,m (**2**) is generally unfavourable but reversible in toluene continuum. Propene insertion involving CIP **2** features uniformly high barriers of 90–100 kJ mol^{-1}, which are much higher than those experimentally observed for MAO-activated catalysts, though the calculated barriers do track with the coordinating ability of the MAO-based anion, as also suggested by the position of the Me$_3$Al-binding equilibria. The binding of the neutral sheet 6,4 to anion [7,4]$^-$ leads to a hybrid anion [13,8]$^-$. The barrier to propene insertion involving CIP SBIZrMe-μ-Me-13,8 (**2e**) is lower than 60 kJ mol^{-1}. Formation of [SBIZrMe$_2$AlMe$_2$][13,8] (**3e**) from SBIZrMe$_2$, 7,5 and 6,4 is favorable, though dissociation into **2e** and $\frac{1}{2}$ Al$_2$Me$_6$ is not. Simulations of catalyst speciation vs. [Al] at constant [Zr] indicate that the formation of species such as **2e** or **3e** from two components of MAO explains the high activity observed for MAO-activated metallocene complexes at sufficiently high Al : Zr ratios. Dedicated to Walter Kaminsky (1941–2024).

Introduction

Methylaluminoxane (MAO)[1] is the most widely used activator for zirconocene-catalyzed olefin polymerization. Its basic mechanism of action is depicted in Scheme 1, illustrated using a particularly well-studied *ansa*-metallocene complex rac-Me$_2$Si(η^5-C$_9$H$_6$)$_2$ZrMe$_2$ (SBIZrMe$_2$). In addition to propene polymerization studies[2] involving both MAO and other activators,[3] NMR spectroscopic techniques have been used to study the activation process,[4] as well as UV-Vis spectroscopy in this specific case.[5] The latter technique shows that at least two contact ion-pairs (CIP) **1** and **2** are formed in varying amounts as a function of the Al : Zr ratio used for catalyst activation. One of these is more prone to form the hetero-dinuclear, outer-sphere ion-pair (OSIP **3**), which is the dominant species present at high Al : Zr ratios.[5] It is known that OSIP **3** and its polymeric analogues are resting states in hexene polymerization using this catalyst.[6]

More recently, the activation of metallocene complexes L$_2$ZrX$_2$ {L$_2$ = Cp$_2$, n-BuCp$_2$, rac-(CH$_2$)$_2$Ind$_2$ (rac-EBI), X = Cl or Me} by MAO using the technique of ESI-MS in fluorobenzene

solvent has been studied.[7] This technique, which selectively detects the cations and anions corresponding to OSIP **3**, complements earlier spectroscopic studies in that the activation of *ansa*-metallocene complexes by MAO is uncomplicated by the formation of homodinuclear [(L$_2$ZrMe)$_2$-μ-X]$^+$ (X = Me, Cl) complexes.[8] Unfortunately, ESI-MS does not provide information about CIP, as the [L$_2$ZrMe]$^+$ cation is only indirectly detected
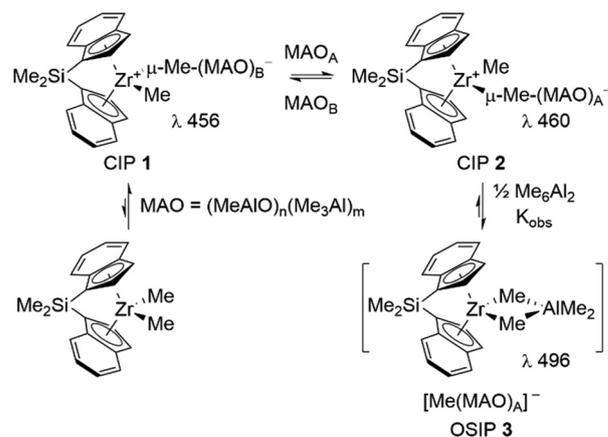
Scheme 1 Activation of SBIZrMe$_2$ by MAO. K_{obs} varies from 2.4 to 6.5 M$^{-\frac{1}{2}}$ between Al : Zr = 100 : 1 to 1000 : 1.[5]

Department of Chemistry, University of Eastern Finland, Joensuu Campus, Yliopistokatu 7, FI-80100 Joensuu, Finland. E-mail: mikko.linnolahti@uef.fi

through the gas-phase, collision-induced dissociation of the $[L_2ZrMe_2AlMe_2]^+$ cation.[9]

However, ESI-MS does provide the m/z ratio of the counter-anions. In the case of hydrolytic MAO from W. R. Grace (10 or 30 wt% solutions and from different batches), a simple negative ion spectrum is obtained using metallocene or other Lewis base donors such as octamethyltrisiloxane (OMTS).[10]

The dominant anion present has m/z 1375, and a likely composition based on MS/MS[10b] is $[(MeAlO)_{16}(Me_3Al)_6Me]^-$ (hereinafter abbreviated $[16,6]^-$) as is illustrated in Fig. 1. Lewis base donors such as OMTS, bipy, pyridine and THF react with h-MAO to provide similar negative ion spectra at additives levels between 0.1–10 mol%.[10a] At higher donor levels the spectra are dominated by many lower m/z anions (<1000 Da).[7c,10]

Interestingly, in the case of metallocenes, higher m/z anions are detected with increased intensity at higher Al:Zr ratios.[7a,b] This observation agrees with previous studies that indicate that ion-pairing is changing in MAO-activated systems.[4,5] If all these anions are formed from precursors, present in fixed amounts in MAO, and via e.g. methide abstraction, one would expect the most Lewis acidic of these to react preferentially with L_2ZrMe_2 at sufficiently high Al:Zr ratios. Conversely, when L_2ZrMe_2 is present in excess of the total amount of available activators, the resulting anion distribution should consist of all species that could possibly form. The exact opposite behavior is seen by ESI-MS,[7a,b] though MAO is a fluxional material, implying a dynamic equilibrium between components of this complex mixture.

Very recently, an active component of MAO $[(MeAlO)_{26}(Me_3Al)_9]$ (hereinafter 26,9) has been isolated and structurally characterized.[11] The structure is analogous to sheet structures[12] we have studied as activators by DFT for the past

several years[7a,b,10,13] and which can form anions $[n,m]^-$ through the process of either methide or $[Me_2Al]^+$ abstraction.[14] However, the $[26,8]^-$ anion that could form from this sheet[11] is a minor component[15] of the mixture of anions that is formed from commercial MAO and 2.0 mol% OMTS (Fig. 1), the same additive used to form a concentrated, liquid clathrate phase[16] from which neutral sheet 26,9 crystallized. The activity of the isolated 26,9 sheet for metallocene-catalyzed olefin polymerization was somewhat more effective than bulk MAO itself at the same Al:Zr ratio.[11]

We recently examined the activation of $SBIZrMe_2$ using DFT methods and sheet 16,6.[17] We found that the free energy difference (ΔG-qh-tr: corrected using a quasi-harmonic method for low energy vibrations,[18] and for the reduced entropy in the condensed phase[19]) between CIP SBIZrMe-μ-Me-16,6 (three isomers) and OSIP [SBIZrMe_2AlMe_2][16,6] (3 three isomers) was in reasonable agreement with experiment[5] at MN15[20]/def2-TZVP[21] level of theory in toluene continuum.[22] This suggested CIP SBIZrMe-μ-Me-16,6 could correspond to CIP 2 in Scheme 1. However, the quasi-harmonic approximation, which involves raising all lower energy vibrations to a threshold of 100 cm^{-1} leads to a significant and variable decrease in the calculated TS-qh-tr and thus we cannot accurately calculate G.[23]

However, we found that propene insertion into the Zr–Me bond of CIP SBIZrMe-μ-Me-16,6 2a had a high electronic and free energy barrier at M06-2X[24]/TZVP[25] in toluene continuum or using a smaller 10,5 model for 16,6, at DLPNO-CCSD(T)[26] level in the gas phase. Since M06-2X/TZVP and DLPNO-CCSD(T) results for SBIZrMe-μ-MeB(C_6F_5)_3, and [SBIZrMe][B(C_6F_5)_4] were in reasonable agreement with the experiment,[2] while those for CIP 2a were not, we were forced to conclude that 2a corresponded to the less reactive ion-pair 1 in Scheme 1, begging the question as to what was the more reactive species.

In this paper, we examine the insertion reactivity of sheet-based ion-pairs as a function of their size, including that derived from the recently isolated 26,9 neutral and propose a different mechanism for catalyst activation that accounts for the behavior of bulk MAO, especially at higher Al:Zr ratios typical of experiments in solution.

Fig. 1 Negative ion ESI-MS spectra of 30 wt% hydrolytic MAO (W. R. Grace Me:Al 1.60:1) and 2.0 mol% OMTS in fluorobenzene with assignments $[n,m]^-$ based on MS-MS. The inset shows the same spectrum with $[16,6]^-$ as the base peak.

Results and discussion

Propene insertion involving aluminoxane sheets

In this paper, we consider CIP 2 and OSIP 3 formed from small sheets $(MeAlO)_n(Me_3Al)_m$ (n = 6–7, m = 4–5)[27] vs. larger sheets 16,6 and 26,9. Sheet 6,4 has a reactive OAlMe_2 group and thus is analogous to 16,6 in forming ion-pair 2 by methide abstraction (Scheme 2). Both ion-pairs feature a chelated counter-anion (see ESI, Table S1.xyz† for structures).

In contrast, 7,5 and 26,9 react via $[Me_2Al]^+$ abstraction and furnish OSIP 3b and 3d; these would be in equilibrium with CIP 2b and 2d through reversible dissociation of Me_3Al (Scheme 2). In these two cases, many structures are possible for CIP 2. We located these by examining electrostatic potential
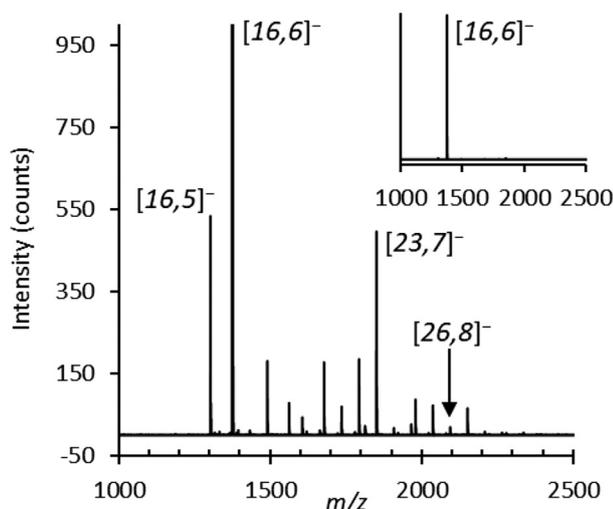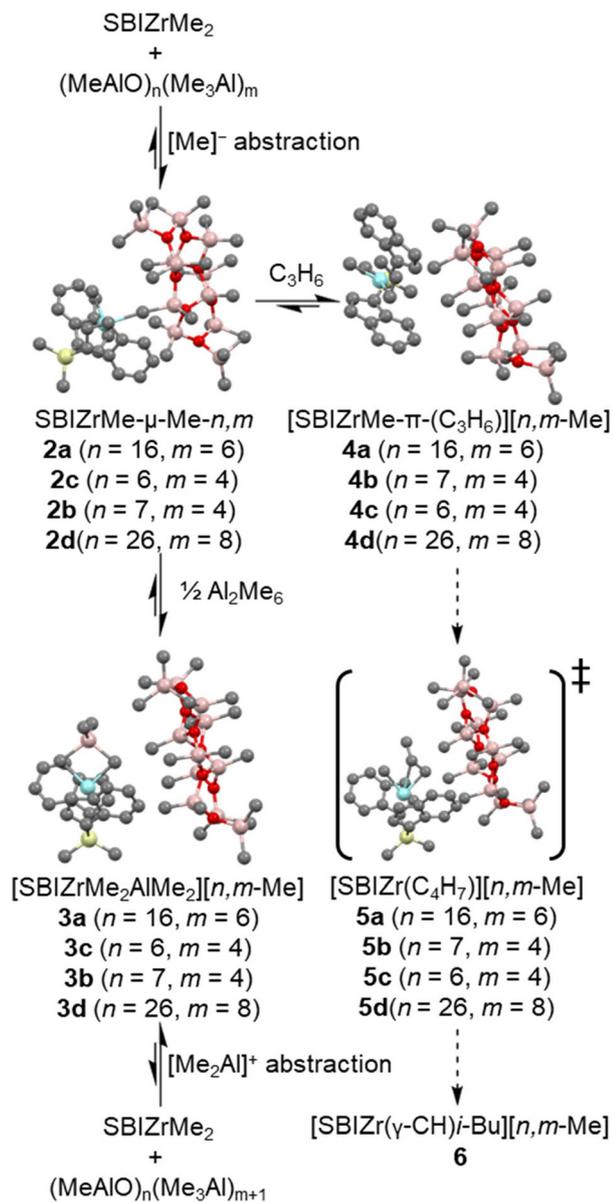
Scheme 2 Catalyst activation and insertion involving SBIZrMe$_2$ and sheet models for MAO. The structures depicted correspond to **2b–5b** with H-atoms omitted for clarity (Zr cyan, Si yellow, Al pink, O red, and C gray).

maps (ESI, Fig. S1 to S3†) of the corresponding sheet anion (usually one face is more electron-rich than the other) and focusing on those O$_2$AlMe$_2$ groups with the highest excess electron density. In practice, the [SBIZrMe]$^+$ cation was then placed above the most electron-rich face within van der Waals contact with one or more these groups. The resulting stationary point might not be the lowest E isomer, but this would not change the conclusions, just serve to increase the height of the insertion barrier. The equilibria between **2** and **3** and neutral starting materials are important with respect to catalyst speciation prior to polymerization. We will discuss the energetics

later in connection with the modeling of the catalyst activation behavior.

An important question is which of these ion-pairs **2** are the most reactive towards olefin insertion. This can be studied at the M06-2X/TZVP level of theory, as in our previous study[17] and other studies of olefin insertion.[28] Ion-pairs **2** will be in pre-equilibrium with the corresponding π complexes **4**, which can form *via* the approach of the monomer *syn* or *anti* to the counter-anion. In earlier work involving **2a**, we showed that the *syn* isomer was more stable than the *anti* and featured a low uptake barrier[17] and so focused on that isomer here when it comes to the location of complexes **4**.

Similarly, the insertion transition state **5** was located *via* rotation of the coordinated propene into the equatorial plane followed by linear transit calculations constraining the Zr–Me···CH(Me)=CH$_2$ distance; frequency calculations were used to confirm the nature of the resulting stationary point, while the imaginary vibration invariably corresponded to the formation of the new C–C bond.

An issue that arises in connection with **4** and **5** is that both are OSIP with different possible orientations of the cation with respect to the anion. We investigated isomers at HF/3-21G* level of theory,[29] fixing the Zr–Me···CH(Me)=CH$_2$ distance in the case of transition structures **5**. Generally, the cation prefers to align along one face of the sheet anion, while the orientation of the cation with respect to this face is usually less important ($\Delta E < 10$ kJ mol^{-1}).

In this work, we deal with the lowest E conformer of those examined, even though one expects several lower E conformers to contribute to the free energy of various processes. In the future, we plan to see if any of these large systems can be investigated by molecular dynamics;[30] the smallest system investigated here SBIZrMe-μ-Me-6,4 still has over 300 valence electrons and no MM force field for the aluminoxanes exists, precluding QM/MM approaches.[31] For the largest structures featuring the [26,8]$^-$ sheet anion, geometry optimizations at M06-2X/TZVP level required typically 1–3 weeks of computing time on 40 processors, even if starting from an optimized M06-2X/SV(P)[32] geometry while a frequency calculation at M06-2X/TZVP level also required about a week of CPU time.

The insertion energetic data are summarized in Table 1 including that previously reported for 16,6.[17] The insertion barrier $\Delta G^{\ddagger}$-qh-tr = 100.3 kJ mol^{-1} is relative to the separated CIP **2a** and C$_3$H$_6$. CIP **2b** is slightly less reactive ($\Delta G^{\ddagger}$-qh-tr = 105.8 kJ mol^{-1}) while CIP **2c** and **2d** are more reactive with $\Delta G^{\ddagger}$-qh-tr = 93.7 and 91.0 kJ mol^{-1}, respectively. All these species are significantly less reactive than either [SBIZrMe][B(C$_6$F$_5$)$_4$] or even SBIZrMe-μ-MeB(C$_6$F$_5$)$_3$ for which the calculated insertion barriers are 58.7 and 77.9 kJ mol^{-1}, respectively for the first insertion.[17] In contrast, the experimental barriers are comparable; 69–72 *vs.* 76–79 kJ mol^{-1} for the 1st insertion step for borate *vs.* MAO (at 2400 : 1 Al : Zr)[2b] and borate = 51–57, borane = 59–67, and MAO = 60–66 kJ mol^{-1} for the subsequent insertions.[2b,c]

It is tempting to blame the discrepancy between theory and experiment on the calculation of $T\Delta S$, especially for the alumi-

Table 1 Energetics of propene insertion for SBIZrMe-μ-X ion-pairs **2** in toluene continuum at 298 K[a]

Structure	ΔE	ΔH	ΔH-qh[b]	$T\Delta S$-tr[b]	$T\Delta S$-qh-tr[b]	ΔG-qh-tr[b]
2a + C$_3$H$_6$ (X = Me-16,6)	0.0	0.0	0.0	0.0	0.0	0.0
4a (π-C$_3$H$_6$) syn	−9.4	−0.5	−2.6	−31.5	−36.5	33.8
5a TS$_i$ syn	47.5	55.8	54.3	−41.6	−46.0	100.3
6a-i-Bu (γ-CH)	−21.7	−6.3	−9.4	−38.9	−43.2	33.9
2b + C$_3$H$_6$ (X = Me-7,4)	0.0	0.0	0.0	0.0	0.0	0.0
4b (π-C$_3$H$_6$) syn	−2.3	6.8	4.2	−35.1	−35.3	39.5
5b TS$_i$ syn	57.7	66.2	63.3	−34.7	−42.5	105.8
2c + C$_3$H$_6$ (X = Me-6,4)	0.0	0.0	0.0	0.0	0.0	0.0
5c TS$_i$ syn	49.0	56.2	52.3	−29.2	−41.4	93.7
2d + C$_3$H$_6$ (X = Me-26,8)	0.0	0.0	0.0	0.0	0.0	0.0
5d TS$_i$ syn	38.9	47.0	45.3	−49.2	−45.7	91.0
2e + C$_3$H$_6$ (X = [7,4-μ-Me-6,4]$^-$ = [13,8]$^-$)	0.0	0.0	0.0	0.0	0.0	0.0
4e (π-C$_3$H$_6$) syn	−30.9	−28.9	−34.0	−26.2	−32.3	−1.7
5e TS$_i$ syn	16.4	22.3	17.6	−29.8	−40.8	58.4
6e-i-Bu (γ-CH)	−22.2	−11.3	−16.7	−24.2	−37.0	20.3

^{a} Energies (kJ mol^{-1}) at the M06-2X/TZVP level are with respect to CIP **2** + C$_3$H$_6$. ^{b} Enthalpy, entropy and free energy corrected using a quasi-harmonic (qh) approximation for low energy vibrations and restricted translational (tr) entropy in the condensed phase.

noxanes, which have disproportionately more low energy vibrations that make a large contribution to the vibrational entropy.[23] However, $T\Delta S^{\ddagger}$-qh-tr values vary by ±3σ = 6.0 kJ mol^{-1} including those for the boron-based activators (Table 2). There is a larger variation seen in the uncorrected $T\Delta S^{\ddagger}$-tr values while the largest deviation between $T\Delta S^{\ddagger}$-qh-tr and $T\Delta S^{\ddagger}$-tr is seen for the aluminoxanes with $T\Delta\Delta S^{\ddagger}$ = 7.1 ± 3.8 kJ mol^{-1}.

There is a weak correlation between $T\Delta S^{\ddagger}$-qh-tr or $T\Delta S^{\ddagger}$-tr and size for the aluminoxanes. This suggests that $T\Delta S^{\ddagger}$ either scales with the molecular size or is being over-estimated for the larger aluminoxanes but by ≤6.0 kJ mol^{-1}. Thus, our calculated barriers may be in error for the aluminoxanes but not to the degree where these would be as reactive as borane or borate.

As for sheet 26,9 we note that this pure compound was not much more reactive than bulk MAO itself and at the same Al : Zr ratio (100–200 : 1).[11] In the case of bulk MAO, only 1–2 mol% of total Al could have been present as an activator in these experiments, implying that whatever is responsible for consumption of monomer is 1–2 orders of magnitude more

reactive than what is formed in the presence of an excess (ca. 3–6 equiv. at 100–200 : 1) of purified 26,9.

As for other forms of MAO, our previous theoretical work on larger, isomeric cages vs. sheets suggests increased stability and reactivity for the latter.[12,33] Moreover, the insertion barrier for the less stable [16,6]$^-$ cage anion was even higher than that seen for the [16,6]$^-$ sheet anion (ESI, Table S1,† $\Delta G^{\ddagger}$-qh-tr = 126.3 kJ mol^{-1}).

Propene insertion involving two different aluminoxane sheets

Since none of the CIP **2** we have investigated had low barriers to insertion, and all were higher than that seen for 26,9, we conclude that at least some of the *individual* components of MAO cannot account for the observed high activities, especially at higher Al : Zr ratios in solution.

Electrostatic potential maps of these anions indicate significant charge dispersal, especially for the larger sheets (ESI†). However, O$_2$AlMe$_2$ or OAlMe$_3$ moieties with terminal AlMe groups still bear an excess of negative charge and are not sterically hindered when it comes to coordination to Zr to form CIP **2**. Thus, these anions are too nucleophilic and form relatively stable CIP **2**, and this accounts for the low insertion reactivity of these species.

The reversible formation of OSIP **3** provides a mechanism for exposing these nucleophilic anions and we wondered whether a coordinating anion could be reversibly trapped through a reaction with excess neutral activators such as 16,6 or 6,4 to furnish a more weakly coordinating anion, especially at higher Al : Zr ratios.

This idea has precedent in the case of discrete activators such as Al(C$_6$F$_5$)$_3$ and Me$_2$AlF,[34] while the effect of charge dispersal is well known for trityl activators with di- vs. mononuclear anions.[3,35] However, in the specific case of MAO, the idea has also been discounted, see the discussion in ref. 4d, which was also accepted in a more recent, comprehensive study of MAO.[36]

Table 2 Entropies of [SBIZrMe(C$_4$H$_9$)][X] transition structures **5** in toluene continuum at 298 K[a]

[X]	ΔE	$T\Delta S^{\ddagger}$-tr	$T\Delta S^{\ddagger}$-qh-tr	$T\Delta\Delta S^{\ddagger b}$
[MeB(C$_6$F$_5$)$_3$]$^-$	27.9	−46.5	−44.6	1.9
[6,4]$^-$	57.7	−34.7	−42.5	−7.8
[B(C$_6$F$_5$)$_4$]$^-$	−6.8	−41.9	−46.2	−4.3
[7,4]$^-$	49.0	−29.2	−41.4	−12.2
[16,6]$^-$	47.5	−41.6	−46.0	−4.4
[26,8]$^-$	38.9	−49.6	−45.7	3.9
Average ± σ	—	−40.6 ± 7.5	−44.4 ± 2.0	7.1 ± 3.8^c

^{a} Energies (kJ mol^{-1}) at M06-2X/TZVP level are with respect to CIP **2** + C$_3$H$_6$. ^{b} $T\Delta\Delta S^{\ddagger}$ = $T\Delta S^{\ddagger}$-qh-tr − $T\Delta S^{\ddagger}$-tr. ^{c} Average is for the aluminoxanes.

We investigated this possibility using the $[7,4]^-$ anion and the neutral 6,4 sheet. The 6,4 neutral has a Lewis acidic $OAlMe_2$ site and it forms a stable donor–acceptor adduct with the $[7,4]^-$ anion (ΔG-qh-tr = -14.5 kJ mol^{-1} in toluene continuum), resulting in a hybrid $[13,8]^-$ anion. Though the composition of this hybrid anion is different from that of *e.g.* $[16,6]^-$, it is similar to both components that have been detected in MAO.[27] Similar cooperative effects could operate between activators such as 26,9 and 16,6; calculations this size will require a supercomputer, something we intend to pursue in the future.

In this hybrid anion, the formal anionic moiety is a sheet-$OAlMe_2$-μ-Me-$AlMeO_2$-sheet group, with a linear Al-μ-Me-Al geometry, which is partially shielded by each sheet from interacting easily with a Zr centre. However, it is still possible for the $SBIZr^+Me$ cation to bind to this hybrid anion through another, more distant O_2AlMe_2 group and CIP **2e**, an isomer favoured by electrostatics and located in the same manner as **2b** and **2d**, is shown in Fig. 2.

The formation of the *syn* **4e** π complex from CIP **2e** (Fig. 2) is expected to be freely reversible with a low barrier based on their similar ΔG-qh-tr values (Table 1) and studies of the uptake barrier in the case of ion-pair **2a**.[17] In fact, the formation of **4e** features a larger electronic stabilization compared with **4a** (or **4b**) and by more than 20 kJ mol^{-1} (Table 1). The cation in **4e** is involved in dispersive, non-bonded interactions with the 7,4 sheet (on the right-hand side of the anion, Fig. 2) but, notice that the formal anionic moiety is quite far removed from the metal centre in this stable intermediate. The insertion barrier featuring this hybrid anion is much lower than that seen for the $[26,8]^-$ or $[16,6]^-$ anion, and based on $\Delta G^{\ddagger}$-qh-tr = 58.4 kJ mol^{-1} is competitive with that seen for $[SBIZrMe][B(C_6F_5)_4]$.

After insertion, the kinetic product features the γ-CH agnostic structure **6e** but notice how the cation has reoriented with respect to the anion with the formal anionic moiety now behind the Me_2Si bridge and unable to easily interact with the metal centre.[37] We expect that further insertion involving this intermediate would be facile and wonder whether binding and insertion of the monomer would be competitive with collapse to form homologated CIP **7e**-i-Bu (ΔG-qh-tr = -47.2 kJ mol^{-1}) and then ultimately, reversible anion dissociation to generate **7b**-i-Bu (dormant in comparison to **7e**-i-Bu) and 6,4. The involvement of transient species such as **2e** *vs.* **2b** could account for intermittent *vs.* continuous propagation behavior[38] invoked for some metallocene catalysts.

Hybrid *vs.* conventional ion-pair formation from aluminoxane sheets 6,4 and 7,5

Though the ion-pair **2e** is much more reactive we wondered to what extent hybrid ion-pair formation would occur in solution simply by changing the Al : Zr ratio. To study this, we investigated the formation of ion-pairs **2b–c** *vs.* **2e** and their Me_3Al adducts **3b–c** *vs.* **3e** at MN15/def2-TZVP level to properly treat covalent *vs.* dispersive interactions in CIP **2** *vs.* OSIP **3**.[39] The results are summarized in Table 3. The formation of ion-pair **2c** is more favorable than **2e** (entry 1 *vs.* 2). The formation of **2e** is favored by both ΔE and ΔH-qh but is accompanied by a large, $-T\Delta S$-qh-tr term as this two-step reaction features three reactant molecules. However, the analogous formation of ion-pair **3e** is more favorable than the formation of **3b** (entry 3 *vs.* 4), despite the higher $-T\Delta S$-qh-tr. Dissociation of ion-pair **3** into **2** and monomeric Me_3Al is unfavorable for all species, though theory predicts that ion-pair **3b** would be the most dissociated in solution (entries 6–8). This along with the insertion barriers (*vide supra*) suggests that of the three anions, the $[7,4]^-$ anion is most strongly coordinating.

To model catalyst speciation, we invoked the mechanism shown in Scheme 3. We propose that the total activator con-
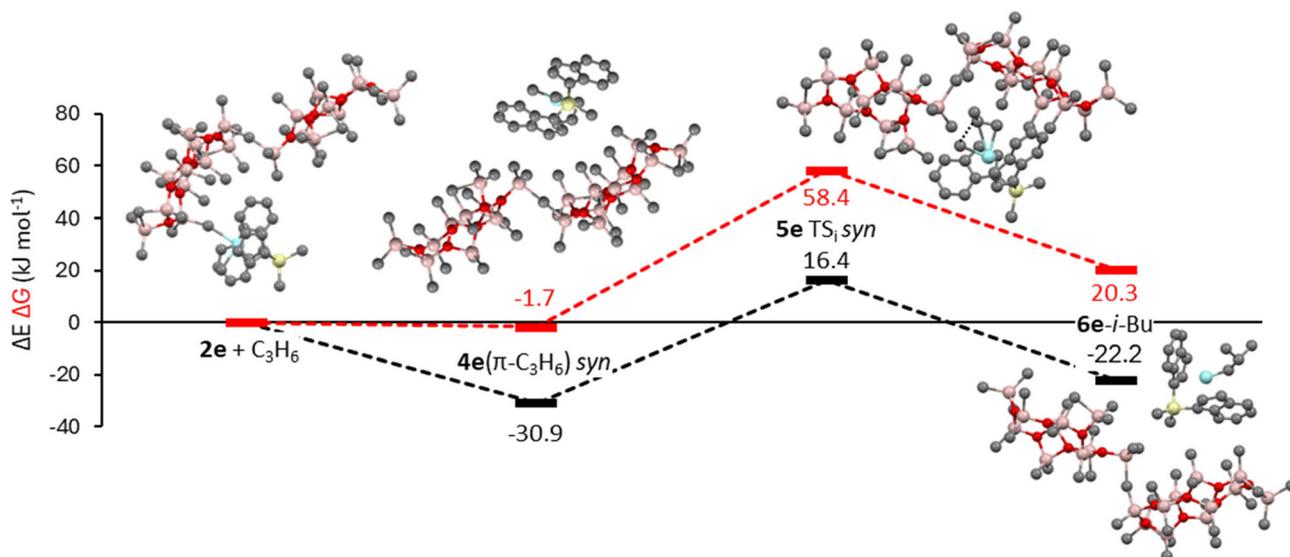

Fig. 2 Reaction coordinate for *syn* insertion of propene into SBIZrMe-μ-Me-13,8.

Table 3 Energetics of ion-pair formation[a]

Entry	Reaction	ΔE	ΔH-qh	ΔG-qh-tr	K_{eq}
1	SBIZrMe$_2$ + 6,4 ⇔ SBIZrMe-μ-Me-6,4 (**2c**)	−83.0	−78.4	−15.4	502 M^{-1}
2	SBIZrMe$_2$ + 6,4 + 7,5 ⇔ SBIZrMe-μ-Me-13,8 (**2e**) + ½ Al$_2$Me$_6$	−89.6	−87.1	6.2	0.082 M$^{-3/2}$
3	SBIZrMe$_2$ + 7,5 ⇔ [SBIZrMe$_2$AlMe$_2$][7,4] (**3b**)	−46.3	−49.4	4.5	0.161 M^{-1}
4	SBIZrMe$_2$ + 6,4 + 7,5 ⇒ [SBIZrMe$_2$AlMe$_2$][13,8] (**3e**)	−132.6	−129.9	−9.5	46 M^{-2}
5	[SBIZrMe$_2$AlMe$_2$][7,4] + 6,4 ⇔ [SBIZrMe$_2$AlMe$_2$][13,8] (**3e**)	−82.2	−79.5	−11.5	101 M^{-1}
6	**3b** ⇔ SBIZrMe-μ-Me-7,4 (**2b**) + Me$_3$Al	57.5	50.7	3.8	0.213 M
7	[SBIZrMe$_2$AlMe$_2$][6,4] (**3c**) ⇔ **2c** + Me$_3$Al	83.2	77.7	29.8	6.2 × 10^{-6} M
8	**3e** ⇔ SBIZrMe-μ-Me-13,8 (**2e**) + Me$_3$Al	92.3	87.3	38.4	1.92 × 10^{-7} M
9	Al$_2$Me$_6$ ⇔ 2 Me$_3$Al	99.5	89.0	45.4	1.15 × 10^{-8} M

[a] Energy differences at MN15/def2-TZVP level in toluene PCM at 298.15 K in kJ mol^{-1}.
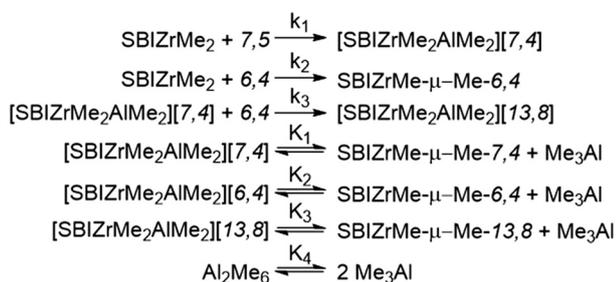
Scheme 3 Activation mechanism.

centration is 1.0 mol% of MAO and in this example, the concentration of 6,4 = 7,5 = 0.005 × [Al], with a total Me$_3$Al content of 15 mol% as is found in MAO from W. R. Grace.[10] We then used COPASI[40] to numerically simulate equilibrium concentrations, requiring the barriers to conversion between different species were all low such that equilibrium was rapidly established.

Though the DFT results indicate that the activation steps are all reversible, simulations that included reversibility based on the ΔG-qh-tr for the different products, as indicated in Table 3, resulted in the reversible formation of SBIZrMe-μ-Me-7,4 (**2b**) under all conditions, with minor amounts of SBIZrMe-μ-Me-6,4 (**2c**) and its Me$_3$Al adduct **3c** (Table 4, entries 1 and 2).

This is because the dissociation of Me$_3$Al from the primary kinetic product [SBIZrMe$_2$AlMe$_2$][7,4] (**3b**) is the least unfavorable of the dissociation equilibria (Table 3, entries 6–8) so that

the overall rate and extent of formation of **2b** with $k_{obs} = (k_1 K_1 / k_1 + k_{-1})[Zr]$ (with $k_1 \sim k_{-1}$) is much greater than any other competing sequence of steps.

Even at a ratio of Al : Zr = 1000 : 1, the formation of **2b** and other products does not proceed to completion with 6,4 and 7,5 present in equal amounts at 0.5 mol% of total Al (a 10-fold excess of activator over added Zr). Only 42–44 mol% of SBIZrMe$_2$ would be converted into ion-pairs (Table 4, entries 1 and 2).

Since this does not reflect actual activation behavior (*i.e.* complete at *ca.* 100 : 1 Al : Zr ratios), we decided to treat all activation steps as quasi-irreversible ($k_{-i} = 0.001$ s^{-1}) but preserved the rate differences. This resulted in nearly quantitative but transient formation of **2c** and its Me$_3$Al-adduct **3c** (total *ca.* 97%), followed by slower conversion to mainly **2b** at equilibrium (Table 4, entries 3 and 4).

Evidently, the formation of SBIZrMe-μ-Me-13,8 (**2e**) would not occur to a significant extent based on our DFT energetics. In essence, the two conventional activation steps must occur at comparable rates, with the resulting ion-pairs having similar Me$_3$Al dissociation constants to generate appreciable amounts of a hybrid ion-pair.

However, given the difference in insertion barriers, ~0.66 ppm levels of **2e** would be as reactive as **2c** (5 ppb levels of **2e** with respect to **2b**). These concentrations are exceeded with [**2e**] ≈ 1 × 10^{-4}[**2c**] in Table 4 (entries 3 and 4) indicating the polymerization kinetics would be dominated by **2e**.

For the sake of completeness, we also modeled a *hypothetical* system in which all activation steps occurred at similar

Table 4 Summary of COPASI modeling results – catalyst speciation (%)[a]

Entry	Al : Zr	k_1 (M^{-1} s^{-1})	K_1 (M)	k_2 (M^{-1} s^{-1})	K_2 (10^{-6} M)	k_3 (M^{-1} s^{-1})	K_3 (10^{-7} M)	K_4 (10^{-8} M)	2e	2c	2b	3e	3c	3b	SBIZrMe$_2$
1	500	0.161[b]	0.213[c]	502[b]	6.2[c]	101[b]	1.92[c]	1.15[c]	3.0 × 10^{-7}	2.5	37.9	6.0 × 10^{-6}	1.6	6.9 × 10^{-4}	58.0
2	1000	0.161[b]	0.213[c]	502[b]	6.2[c]	101[b]	1.92[c]	1.15[c]	3.1 × 10^{-7}	2.4	39.9	6.4 × 10^{-6}	1.5	7.3 × 10^{-4}	56.1
3	500	0.161[d]	0.213[c]	502[d]	6.2[c]	101[d]	1.92[c]	1.15[c]	6.7 × 10^{-4}	7.4	87.8	1.4 × 10^{-2}	4.6	1.6 × 10^{-3}	0.18
4	1000	0.161[d]	0.213[c]	502[d]	6.2[c]	101[d]	1.92[c]	1.15[c]	7.0 × 10^{-4}	6.1	89.9	1.4 × 10^{-2}	3.8	1.6 × 10^{-3}	0.14
5	500	161[d]	1.92 × 10^{-6c}	502[d]	1.92[c]	101[d]	1.92[c]	1.15[c]	1.9	16.6	3.3	37.6	33.4	6.6	0.59
6	1000	161[d]	1.92 × 10^{-6c}	502[d]	1.92[c]	101[d]	1.92[c]	1.15[c]	2.0	16.0	2.8	40.8	32.3	5.6	0.44

[a] [SBIZrMe$_2$]$_0$ = 1.75 or 3.5 × 10^{-5} M with [Al] = 0.0175 M, [7,5] = [6,4] = 8.75 × 10^{-5} M, [Al$_2$Me$_6$] = 1.3125 × 10^{-3} M. Highlighted in red are major species present at equilibrium. [b] Reverse reaction with $k_{-i} = 0.1$ s^{-1}. [c] Reverse reaction-diffusion controlled with $k = 10^{10}$ M^{-1} s^{-1}. [d] Reverse reaction with $k_{-i} = 0.001$ s^{-1}.
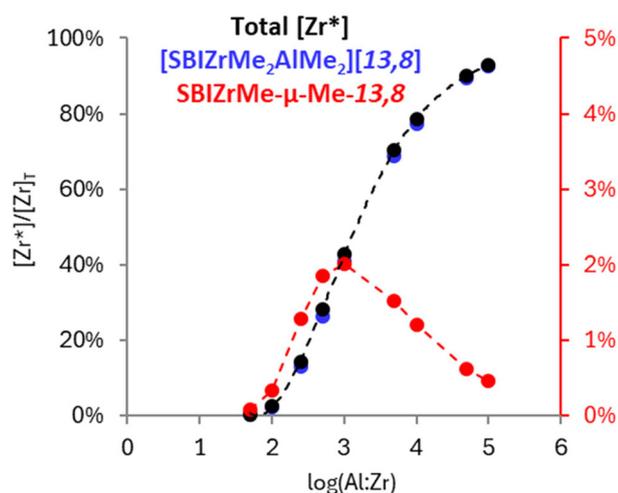
Fig. 3 SBIZrMe$_2$-13,8 (**2e** + **3e**) catalyst speciation *vs.* Al:Zr ratio as simulated using COPASI.[40] The percentages of **2e** and **3e** were determined using COPASI simulations at different [Al] concentrations using the final rate and equilibrium constants (Table 4, entries 5 and 6). Data in red are plotted along the right-hand axis.

rates, while the Me$_3$Al dissociation steps involving **3c** and **3b** were identical but more favorable than for **3e** such that no one product dominated (Table 4, entries 5 and 6).

Under the assumption that only the ion-pair **2e** featuring the hybrid anion is reactive towards insertion, active site concentrations [Zr*] = [**2e**] + [**3e**] as a function of the Al:Zr ratio at fixed [Zr] = 1.75×10^{-5} M for this scenario are shown in Fig. 3.

The overall features can be understood in terms of two competing factors – an increase in the relative amount of the active catalyst (**2e** + **3e**) with increasing Al:Zr ratios *vs.* an increasing amount of the dormant state [SBIZrMe$_2$AlMe$_2$][13,8] (**3e**) with increasing [Al] at constant [Zr]. Note that the specific features shown in Fig. 3 concur with the experimental data on both propene polymerization (bell-shaped polymerization rate data at constant [Zr])[2f] and catalyst activation (*i.e.* saturation) behavior in the case of the SBI complex.[5] In this hypothetical case the amount of the active catalyst **2e** never exceeds 3 mol% of total Zr under all conditions. This is in good agreement with estimates of active site concentration (*ca.* 8 mol%) determined from the kinetics of propene polymerization involving SBIZrMe$_2$ and MAO (2400 : 1).[2a,b]

Although the agreement in this example is deliberate, our modeling results do indicate that [Me$_2$Al]$^+$ and [Me]$^-$ abstraction would have to occur at competitive rates and that both types of activators would have to be present in comparable amounts to account for actual polymerization behavior.

Conclusions

We have shown in this paper that the reactivity of aluminoxane sheets is indeed size-dependent, though not in the expected way. For example, a lower MW 6,4 activator is more reactive

towards methide abstraction than 16,6, while the converse is true when it comes to [Me$_2$Al]$^+$ abstraction and 7,5 *vs.* 26,9. These differences are easy to understand. The former process involves the Lewis acidity of the specific site and the stability of the resulting CIP. In contrast, [Me$_2$Al]$^+$ abstraction leads directly to an OSIP and so it is the weakly coordinating nature of the anion that is most important here.

Insertion barriers correlate with the latter aspect since the transition structure **5** is also an OSIP, though one should bear in mind that those barriers are relative to CIP **2** and so the stability of the latter (relative to reactive neutrals) is also important. We believe this feature contributes to the high energy barriers in the case of CIP **2a–d**. We do note that the intermediate π complex **4** is also an OSIP and that it is often lower in *E* than the corresponding CIP + monomer (Table 1). In the case of **2e**, the π complex is actually marginally lower in Δ*G*-qh-tr as noted elsewhere in the case of [SBIZrMe(π-C$_3$H$_6$)][B(C$_6$F$_5$)$_4$].[17] This is likely a pre-requisite for highly active catalysts in that the binding process is largely entropic in nature.[41]

Finally, we have demonstrated that two components of MAO can cooperate to form a weakly coordinating anion and that a process of this sort can account for the exceptionally high activities seen at high Al:Zr ratios in solution for MAO-activated metallocene catalysts. The change in ion-pairing that is known to occur during metallocene catalyst activation, as evidenced by UV-Vis, NMR and ESI-MS (as well as polymerization activity) could have many explanations and ours is a reasonable one. In reality, it is possible that larger sheets such as 16,6 (reactive towards [Me]$^-$ abstraction) and 26,9 (reactive towards [Me$_2$Al]$^+$ abstraction) could cooperate in exactly the same fashion as demonstrated here to produce *transient* species with weakly coordinating anions. Future work should focus on these issues and from a theoretical perspective, understanding the dynamics of these complex molecules would seem to be essential.

Experimental section

Geometry optimizations and electronic energy calculations were performed using the M06-2X density functional, in conjunction with the TZVP basis set, or using the MN15 density functional in combination with the def2-TZVP basis set. For Zr, a relativistic effective core potential of 28 electrons was used for the description of the core electrons.[42] Polarizable continuum model calculations were employed by the integral equation formalism variant (IEFPCM).[22] Stationary points were confirmed as minima or transition structures by harmonic vibrational frequency calculations using Gaussian 16.[43]

Quasi-harmonic corrections to the entropy[18a] and enthalpy[18b] employed a cut-off frequency of 100 cm^{-1} and the reduced translational entropy in the solution was calculated by the method described by Whitesides and co-workers.[19] All corrections were implemented using the Goodvibes script.[44] A molarity of 9.40 M and a molecular volume of 138.4 Å^3 were used for toluene.

Author contributions

M. L. and S. C. carried out quantum calculations. S. C. carried out the kinetic simulations and both authors co-wrote the manuscript.

Data availability

The data supporting this article are included as part of the ESI.†

Conflicts of interest

There are no conflicts to declare.

Acknowledgements

References

1 Reviews: (a) H. S. Zijlstra and S. Harder, *Eur. J. Inorg. Chem.*, 2015, 19–43; (b) W. Kaminsky, *Macromolecules*, 2012, **45**, 3289–3297.

2 (a) F. Song, R. D. Cannon and M. Bochmann, *Chem. Commun.*, 2004, 542–543; (b) F. Song, R. D. Cannon and M. Bochmann, *J. Am. Chem. Soc.*, 2003, **125**, 7641–7653; (c) J. Zhou, S. J. Lancaster, D. A. Walker, S. Beck, M. Thornton-Pett and M. Bochmann, *J. Am. Chem. Soc.*, 2001, **123**, 223–237 See also: (d) V. N. Panchenko, D. E. Babushkin, J. E. Bercaw and H.-H. Brintzinger, *Polymers*, 2019, **11**, 936 (e) B. M. Moscato, B. Zhu and C. R. Landis, *Organometallics*, 2012, **31**, 2097–2107 for studies of 1-hexene polymerization. For the original kinetic study of SBIZrCl$_2$/MAO at room temperature see. (f) N. Herfert and G. Fink, *Makromol. Chem.*, 1992, **193**, 1359–1367.

3 Reviews: (a) F. Zaccaria, L. Sian, C. Zuccaccia and A. Macchioni, in *Advances in Organometallic Chemistry*, ed. P. J. Perez, Academic Press, Cambridge, MA, 2020, vol. 73, ch. 1; (b) M. Bochmann, *Organometallics*, 2010, **29**, 4711–4740; (c) E. Y.-X. Chen and T. J. Marks, *Chem. Rev.*, 2000, **100**, 1391–1434.

4 (a) D. E. Babushkin, C. Naundorf and H. H. Brintzinger, *Dalton Trans.*, 2006, 4539–4544; (b) l. Schröder, H. H. Brintzinger, D. E. Babushkin, D. Fischer and R. Mülhaupt, *Organometallics*, 2005, **24**, 867–871; (c) K. P. Bryliakov, N. V. Semikolenova, D. V. Yudaev, V. A. Zakharov, H. H. Brintzinger, M. Ystenes, E. Rytter and E. P. Talsi, *J. Organomet. Chem.*, 2003, **683**, 92–102; (d) D. E. Babushkin and H. H. Brintzinger, *J. Am. Chem. Soc.*, 2002, **124**, 12869–12873; (e) D. E. Babushkin, N. V. Semikolenova, V. A. Zakharov and E. P. Talsi, *Macromol. Chem. Phys.*, 2000, **201**, 558–567; (f) I. Tritto, R. Donetti, M. C. Sacchi, P. Locatelli and G. Zannoni, *Macromolecules*, 1997, **30**, 1247–1252.

5 (a) U. Wieser, F. Schaper and H. H. Brintzinger, *Macromol. Symp.*, 2006, **236**, 63–68; (b) U. Wieser and H.-H. Brintzinger in *Organometallic Catalysts and Olefin Polymerization*, ed. R. Blom, A. Follestad, E. Rytter, M. Tilset and M. Ystenes, Springer, Berlin, 2001, pp. 3–13; (c) U. Wieser, *Spektroskopische Untersuchungen an Zirkonocen-Katalysatorsystemen*, UFO, Atelier für Gestaltung und Verl., Allensbach, Germany, 2002, ISBN: 3-935511-17-5.

6 D. E. Babushkin and H. H. Brintzinger, *J. Am. Chem. Soc.*, 2010, **132**, 452–453.

7 (a) S. Collins and M. Linnolahti, *ChemCatChem*, 2022, **14**, e202101918; (b) S. Collins, M. Linnolahti, M. G. Zamora, H. S. Zijlstra, M. T. R. Hernández and O. Perez-Camacho, *Macromolecules*, 2017, **50**, 8871–8884; (c) T. K. Trefz, M. A. Henderson, M. Linnolahti, S. Collins and J. S. McIndoe, *Chem. – Eur. J.*, 2015, **21**, 2980–2991; (d) T. K. Trefz, M. A. Henderson, M. Wang, S. Collins and J. S. McIndoe, *Organometallics*, 2013, **32**, 3149–3152.

8 (a) O. Y. Lyakin, K. P. Bryliakov, N. V. Semikolenova, A. Y. Lebedev, A. Z. Voskoboynikov, V. A. Zakharov and E. P. Talsi, *Organometallics*, 2007, **26**, 1536–1540; (b) K. P. Bryliakov, D. E. Babushkin, E. P. Talsi, A. Z. Voskoboynikov, H. Gritzo, L. Schröder, H. R. H. Damrau, U. Wieser, F. Schaper and H. H. Brintzinger, *Organometallics*, 2005, **24**, 894–904; (c) K. P. Bryliakov, E. P. Talsi and M. Bochmann, *Organometallics*, 2004, **23**, 149–152; (d) M. Bochmann and S. J. Lancaster, *Angew. Chem., Int. Ed. Engl.*, 1994, **33**, 2634–1637.

9 A. Joshi, S. Donnecke, O. Granot, D. Shin, S. Collins, I. Paci and J. S. McIndoe, *Dalton Trans.*, 2020, **49**, 7028–7036.

10 (a) H. S. Zijlstra, A. Joshi, M. Linnolahti, S. Collins and J. S. McIndoe, *Eur. J. Inorg. Chem.*, 2019, 2346–2355; (b) H. S. Zijlstra, M. Linnolahti, S. Collins and J. S. McIndoe, *Organometallics*, 2017, **36**, 1803–1809.

11 L. Luo, J. M. Younker and A. V. Zabula, *Science*, 2024, **384**, 1424–1428.

12 S. Collins and M. Linnolahti, *ChemPhysChem*, 2017, **18**, 3369–3374.

13 (a) S. Collins, G. Hasan, A. Joshi, J. S. McIndoe and M. Linnolahti, *ChemPhysChem*, 2021, **22**, 1326–1335; (b) A. Joshi, S. Collins, M. Linnolahti, H. S. Zijlstra, E. Liles and J. S. McIndoe, *Chem. – Eur. J.*, 2021, **27**, 8753–8763; (c) A. Joshi, H. S. Zijlstra, E. Liles, C. Concepcion, M. Linnolahti and J. S. McIndoe, *Chem. Sci.*, 2021, **12**, 546–551.

14 (a) J. T. Hirvi, M. Bochmann, J. R. Severn and M. Linnolahti, *ChemPhysChem*, 2014, **15**, 2732–2742;

(*b*) M. S. Kuklin, J. T. Hirvi, M. Bochmann and M. Linnolahti, *Organometallics*, 2015, **34**, 3586–3597.

15 One should be careful about discussing ion abundance based on relative intensities in ESI-MS spectra since the latter depend inter alia on *m*/*z* ratio as well as surface activity of the ions in question. See e.g. I. Omari, P. Randhawa, J. Randhawa, J. Yu and J. S. McIndoe, Structure, anion, and solvent effects on cation response in ESI-MS, *J. Am. Soc. Mass Spectrom.*, 2019, **30**, 1750–1757.

16 S. K. Spear, J. D. Holbrey and R. D. Rogers, "Liquid Clathrates" in *Encyclopedia of Supramolecular Chemistry*, ed. J. L. Atwood, CRC Press, 2004, DOI: 10.1201/9780429075728.

17 S. Collins and M. Linnolahti, *ChemPhysChem*, 2024, **25**, e202300856.

18 (*a*) R. F. Ribeiro, A. V. Marenich, C. J. Cramer and D. G. Truhlar, *J. Phys. Chem. B*, 2011, **115**, 14556–14562; (*b*) Y.-P. Li, J. Gomes, S. M. Sharada, A. T. Bell and M. Head-Gordon, *J. Phys. Chem. C*, 2015, **119**, 1840–1850.

19 M. Mammen, E. I. Shakhnovich, J. M. Deutch and G. M. Whitesides, *J. Org. Chem.*, 1998, **63**, 3821–3830.

20 H. S. Yu, X. He, S. L. Li and D. G. Truhlar, *Chem. Sci.*, 2016, **7**, 5032–5051.

21 F. Weigend and R. Ahlrichs, *Phys. Chem. Chem. Phys.*, 2005, **7**, 3297–3305.

22 G. Scalmani and M. J. Frisch, *J. Chem. Phys.*, 2010, **132**, 114110.

23 M. Linnolahti and S. Collins, *Dalton Trans.*, 2022, **51**, 11152–11162.

24 Y. Zhao and D. G. Truhlar, *Theor. Chem. Acc.*, 2008, **120**, 215–241.

25 A. Schäfer, C. Huber and R. Ahlrichs, *J. Chem. Phys.*, 1994, **100**, 5829–5835.

26 C. Riplinger, B. Sandhoefer, A. Hansen and F. Neese, *J. Chem. Phys.*, 2013, **139**, 134101.

27 Both [6,4]⁻ and [7,4]⁻ anions are detected during the hydrolysis of Me₃Al, while the [7,4]⁻ anion is also present at trace levels in commercial MAO. See ref. 10 and 13.

28 (*a*) C. Ehm, P. H. M. Budzelaar and V. Busico, *J. Organomet. Chem.*, 2015, **775**, 39–49; (*b*) A. Laine, B. B. Coussens, J. T. Hirvi, A. Berthoud, N. Friederichs, J. R. Severn and M. Linnolahti, *Organometallics*, 2015, **34**, 2415–2421.

29 M. Linnolahti, P. Hirva and T. A. Pakkanen, *J. Comput. Chem.*, 2001, **22**, 51–64.

30 (*a*) F. De Angelis, S. Fantacci and A. Sgamellotti, *Coord. Chem. Rev.*, 2006, **250**, 1497–1513; (*b*) M. S. W. Chan and T. Ziegler, *Organometallics*, 2000, **19**, 5182–5189.

31 (*a*) C. N. Rowley and T. K. Woo, *Organometallics*, 2011, **30**, 2071–2074; (*b*) A. Correa and L. Cavallo, *J. Am. Chem. Soc.*, 2006, **128**, 10952–10959; (*c*) S.-Y. Yang and T. Ziegler, *Organometallics*, 2006, **25**, 887–900.

32 A. Schäfer, H. Horn and R. Ahlrichs, *J. Chem. Phys.*, 1992, **97**, 2571.

33 S. Collins and M. Linnolahti, *ChemPhysChem*, 2023, **24**, e202300342.

34 (*a*) E. Y.-X. Chen, W. J. Kruper, G. Roof and D. R. Wilson, *J. Am. Chem. Soc.*, 2001, **123**, 745–746; (*b*) L. Oliva, P. Oliva, N. Galdi, C. Pellecchia, L. Sian, A. Macchioni and C. Zuccaccia, *Angew. Chem., Int. Ed.*, 2017, **56**, 14227–14231.

35 M. Delferro and T. J. Marks, *Chem. Rev.*, 2011, **111**, 2450–2485.

36 F. Ghiotto, C. Pateraki, J. Tanskanen, J. R. Severn, N. Luehmann, A. Kusmin, J. Stellbrink, M. Linnolahti and M. Bochmann, *Organometallics*, 2013, **32**, 3354–3362.

37 C. Zuccaccia, N. G. Stahl, A. Macchioni, M.-C. Chen, J. A. Roberts and T. J. Marks, *J. Am. Chem. Soc.*, 2004, **126**, 1448–1464.

38 (*a*) C. R. Landis, K. A. Rosaaen and D. R. Sillars, *J. Am. Chem. Soc.*, 2003, **125**, 1710–1711; (*b*) F. Schaper, A. Geyer and H.-H. Brintzinger, *Organometallics*, 2002, **21**, 473–483; (*c*) G. Fink, W. Fenzl and R. Mynott, *Z. Naturforsch., B:J. Chem. Sci.*, 1985, **406**, 158–166.

39 H. S. Yu, X. He, S. L. Li and D. G. Truhlar, *Chem. Sci.*, 2016, **7**, 5032–5051.

40 S. Hoops, S. Sahle, R. Gauges, C. Lee, J. Pahle, N. Simus, M. Singhal, L. Xu, P. Mendes and U. Kummer, *Bioinformatics*, 2006, **22**, 3067–3074.

41 F. Zaccaria, C. Ehm, P. H. M. Budzelaar and V. Busico, *ACS Catal.*, 2017, **7**, 1512–1519 and references therein.

42 D. Andrae, U. Haeussermann, M. Dolg, H. Stoll and H. Preuss, *Theor. Chim. Acta*, 1990, **77**, 123–141.

43 M. J. Frisch, G. W. Trucks, H. B. Schlegel, G. E. Scuseria, M. A. Robb, J. R. Cheeseman, G. Scalmani, V. Barone, G. A. Petersson, H. Nakatsuji, X. Li, M. Caricato, A. V. Marenich, J. Bloino, B. G. Janesko, R. Gomperts, B. Mennucci, H. P. Hratchian, J. V. Ortiz, A. F. Izmaylov, J. L. Sonnenberg, D. Williams-Young, F. Ding, F. Lipparini, F. Egidi, J. Goings, B. Peng, A. Petrone, T. Henderson, D. Ranasinghe, V. G. Zakrzewski, J. Gao, N. Rega, G. Zheng, W. Liang, M. Hada, M. Ehara, K. Toyota, R. Fukuda, J. Hasegawa, M. Ishida, T. Nakajima, Y. Honda, O. Kitao, H. Nakai, T. Vreven, K. Throssell, J. A. Montgomery Jr., J. E. Peralta, F. Ogliaro, M. J. Bearpark, J. J. Heyd, E. N. Brothers, K. N. Kudin, V. N. Staroverov, T. A. Keith, R. Kobayashi, J. Normand, K. Raghavachari, A. P. Rendell, J. C. Burant, S. S. Iyengar, J. Tomasi, M. Cossi, J. M. Millam, M. Klene, C. Adamo, R. Cammi, J. W. Ochterski, R. L. Martin, K. Morokuma, O. Farkas, J. B. Foresman and D. J. Fox, *Gaussian 16, Revision A.03*, Gaussian, Inc., Wallingford CT, 2016.

44 G. Luchini, J. V. Alegre-Requena, Y. Guan, I. Funes-Ardoiz and R. S. Paton, *GoodVibes, Version 3.0.1*, 2019, https://f1000research.com/articles/9-291/v1.